Cement & Concrete Composites 33 (2011) 402–410

Contents lists available at ScienceDirect

Cement & Concrete Composites

journal homepage: www.elsevier.com/locate/cemconcomp

Free and restrained early-age shrinkage of mortar: Influence of glass fiber, cellulose ether and EVA (ethylene-vinyl acetate)

A. Messan *, P. Ienny, D. Nectoux

Ecole des Mines d'Alès – CMGD, 6 avenue de Clavières, F-30319 Alès cedex, France

ARTICLE INFO

Article history:
Received 26 April 2007
Received in revised form 24 October 2010
Accepted 26 October 2010
Available online 30 October 2010

Keywords:
Mortar
Plastic shrinkage
Cellulose ether
EVA
Glass fibers
Optical instrumentation
Active ring test

ABSTRACT

The objective of this paper is to present a new testing method for investigating early-age (i.e. between 0 and 24 h after mixing) shrinkage of cement-based material. Whatever the free or restrained conditions, the plastic shrinkage is caused by the evaporation of water from the surface of fresh concrete. Free plastic shrinkage was investigated by optical instrumentation system. It can thus be measured the average shrinkage before and/or very early after the setting process. In addition to this value, the optical system provides a measurement of the deformation field to assess the degree of heterogeneity of shrinkage at the surface of the sample during the drying. The restrained shrinkage tests are performed using an active restrained system. The testing apparatus, based on a ring test, is presented with its own computer-controlled closed loop. This technique provides quantitative information about stress development that may be used to assess the potential for cracking in thin cement-based materials subjected to drying. As first results, the influence of the mix design (cellulose ether, EVA and glass fiber) has also been investigated: reducing of cellulose ether quantity in mix-design, modifies the kinetic and level of early-age shrinkage. The use of EVA decreases the overall shrinkage but does not reduce the heterogeneity of surface shrinkage. However we obtained with EVA, a decrease in the internal residual stress. The glass fiber reduces shrinkage and also reduces the heterogeneity of the surface shrinkage. However at a low rate of incorporation of glass fibers, no reduction of internal residual stress is obtained.

1. Introduction

Without any external and thermomechanical sollicitations, the mortar is prone to significant dimensional variation from the first hours after placement. This dimensional variation is commonly called "shrinkage". Under certain conditions (climatic, structural or otherwise) the deformations generated during the early-age shrinkage can lead to the cracking of cementitious structures. Unfortunately, this early-age cracking severely affects large area elements such as slabs, pavements, and industrial, parking lot and garage floors [3,4]. The resulting cracks are sometimes internal and microscopic or sometimes "very open" (i.e. the size of the crack is visible to the human eye [1]). In the latter case, cracking can facilitate the penetration of aggressive agents such as chlorides, sulfates or carbon dioxide inside the structure. This leads to problems of degradation of the cementing matrix containing reinforcing steel, which can compromise the durability of the cement-based material [2]. If the cracks are internal and microscopic, they can lead onto further cracking related to shrinkage after setting time. It is thus imperative to control the early-age shrinkage of cement-based materials. Although it is recognized that the early-age shrinkage is a complex problem, it is usually connected to several factors such as bleeding, cement hydration, water evaporation and to the capillary depression [21]. However, water evaporation remains the principal cause of early-age shrinkage in cement-based materials. The free shrinkage value is commonly used to investigate the tendency for early cracking in cementitious structures [3,7,19].

The objective of this work concerns the early-age shrinkage of thin mortars (such as pavements or facings) under drying conditions. This article investigates the influence of free and restrained conditions on the behavior of mortar in the first period after casting, with a view to the risk of early-age cracking. Because the early-age cracking often appear so early after casting, the period investigated is intentionally limited to the first 24 h of the early-age time.

The experimental procedure combines a free-shrinkage test on slab mortar and an active restraining system based on ring geometry. Firstly we describe the materials and the mix design. Secondly we detail the free and restrained shrinkage tests. Drying shrinkage should be analyzed at the surface in order better to predict free shrinkage cracking because plastic shrinkage is mainly limited to

* Corresponding author.
E-mail addresses: Adamah.Messan@ema.fr (A. Messan), Patrick.Ienny@ema.fr (P. Ienny), Didier.Nectoux@ema.fr (D. Nectoux).

0958-9465/$ - see front matter © 2011 Published by Elsevier Ltd.
doi:10.1016/j.cemconcomp.2010.10.019

the concrete [1]. Unfortunately, existing measurement techniques only give an average value through the thickness of the structure [16,18]. We therefore used optical instrumentation, based on image correlation processing to investigate free early-age shrinkage at the open surface of the sample. This method also gives quantitative information about local concentrations of the shrinkage phenomenon at the mortar surface. In addition to free early-age shrinkage, restrained shrinkage tests need to be carried out in order to establish the damage stress criteria. This paper presents a novel and original device for investigating restrained shrinkage in mortar. We give the equations needed to provide quantitative information about the evolution of the restrained tensile stress in cement-based materials during drying. Then the accuracy of the experimental procedure is analyzed based on calibration and repeatability tests. Finally the effect of glass fibers (GF), cellulose ether (CE) and ethylene-vinyl acetate (EVA) on plastic shrinkage was investigated.

2. Materials

The studies were related to a reference mortar developed in the framework of the Consortium pour l'Etude et la REcherche sur les Mortiers (CEReM) project. Round grain silica sand was used (SIFRACO) with a grading range of 100–350 μm. The cement used was CEM I 52.5N CP2 (EN 197-1) with a specific surface of 438 m^2/kg. Its high C_3S content (71.3%) speeds up hardening. The limestone filler had a grading range and specific surface close to those of the cement, 0–100 μm and 570 m^2/kg respectively. Two types of additions were investigated, AR glass fiber (GF) and admixtures (cellulose ether (CE) and latex (EVA)). The latex was used to substitute of 4.6% of the sand (by weight). CEMFIL HD (high dispersion) AR glass fibers were added to the mortar in the proportion 0.035% by volume, i.e. 1 kg/m^3 of mortar. The characteristics of the AR glass fibers are given in Table 1. Table 2 lists the specimens and their mixture proportions. The values are given compared to the mortar weight. All mortars were prepared using a water–cement ratio $w/c = 1$.

Because the plain mortar was a specific mortar used in the framework of the CEReM project, all the mortars were prepared according to the CEReM recommendations. They were all prepared in a conventional drum mixer at a slow speed. First the cement and other fine particles were mixed for 1 min to preserve the uniformity of the mixture. Then the mixing water was added and then mixed for 2 min. Note that the fibers were added to mixing water to ensure better distribution in the mortar. The tests described below were conducted in an air-conditioned room, where the temperature and relative humidity were 21 ± 1 °C and 50 ± 5% respectively.

3. Experimental set up

3.1. Free plastic shrinkage test: local and global strain measurement

3.1.1. Principle and conditions of test

The device schematized in Fig. 1 was used to determine the free shrinkage at the upper surface of the slab of fresh mortar. The side and the thickness of the molded slab were 500 mm and 15 mm respectively and the interior of the mould was coated with a layer of paint to reduce the friction between the mould and the fresh mortar. The mortar was cast in the mould immediately after mixing. Drying was allowed to occur from the top surface of the specimen and the free shrinkage was assumed to be quasi-homogeneous and uniform throughout the in-plane directions of the open surface.

Table 2
List of specimens and mixture proportion.

CE–EVA–GF	CE weight (%)	EVA weight (%)	GF weight (%)
38–0–0	0.38	0	0
20–0–0	0.20	0	0
20–2–0	0.20	2.3	0
20–0–6	0.20	0	0.06

3.1.2. Image procedure

The evolution of the shrinkage strain was obtained using an optical apparatus. This technique involves the evaluation of the in-plane kinematic surface field without contact with the tested sample. Slowik (2004) and Wong (2007) have already investigated the early-age shrinkage of cement paste and reactive powder concrete, respectively, using fiber Bragg gratings (FBGs): although this method is freely calibrated and enables long-term measurement without drift, it requires analytical compensation of the thermo-optical effect [16,22]. However, the FBG method is not very appropriate to early-age studies because the mix is not generally stiff enough to transfer the strain to the fiber at this stage [22]. We adapted an imaging procedure for the free-shrinkage test in order to quantify the Green Lagrange strain tensor at any point at the top surface of the mortar. The experimental set up consisted of a white-light source associated to the natural signature of the mortar surface, a high resolution Charged coupled device (CCD) camera (KODAK Megaplus 1.4, 1024 × 1024 squared and jointed pixels) positioned vertically and perpendicularly to the surface of the sample (Fig 1). Firstly, images of the successive states of the mortar slab subjected to drying were recorded during the first 24 h. In order to minimize boundary effects, the region of interest (ROI) was located 100 mm (3.937 in) from the edges of the specimen. At this magnification, the images recorded were square with a side of 300 mm (11.811 in) and one pixel represented about 300 μm (1.2×10^{-2} in). The recording of the images began 27 min after the first water-mix contact in order to enable the implementation of the experimental setup, and the frequency was one image per 15 min. Although the mix was obtained using the ratio $w/c = 1$, bleeding was not significant enough to modify the optical measurement.

3.1.3. Computational procedure

Following the test, a pattern matching procedure using image correlation (CinEMA software developed by the Alès School of Mines) was carried out on the recorded sequence of images. The post-processing algorithm used in this study was the version developed and presented by Giton and Laraba-Abbes [5,10]. For the magnification used, these studies shows that post-processing provides an accuracy of 5×10^{-5} with regard to the computed strain. At the first step of the processing operation, virtual points are distributed over the ROI to produce a virtual mesh. The spacing between two points of the virtual grid is 10 pixels (3 mm/0.118 in). The image processing by Digital Image Correlation is

Table 1
Properties and dimensions of AR glass fibers.

Tensile strength (MPa)	Modulus of elasticity (MPa)	Density (kg/m^3)	Diameter (μm)	Length (mm)	Specific surface (m^2/kg)	Number of filaments (per g)
3000	80,000	2600	14	12	110	210,000

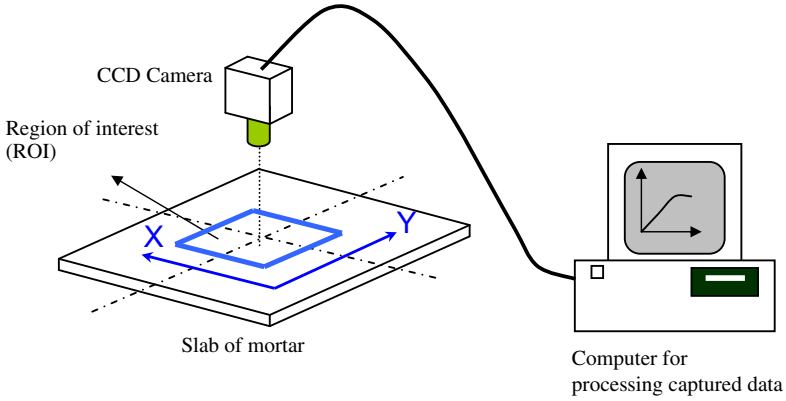

Fig. 1. Schematic description of the free-shrinkage test.

based on a coarse–fine search method leading to the two-dimensional displacement components with subpixel accuracy. Applied to all the points of the virtual mesh, this process provides the increment of the displacement fields between two images. This procedure was applied to the whole set of images recorded during the free-shrinkage test. Finally, for each analyzed point, the in-plane strain tensor is determined by a linear fit of the displacement field gradient obtained for the immediate neighbors of the point of interest. This is performed by selecting a given number of digital patterns surrounding the subset of interest. An equivalent gauge's length could be defined by the distance between the farthest points surrounding the considered pattern. By using all the points defined on the virtual grid to determine the in-plane strain tensor, it is possible to calculate the average of the plane tensor on the ROI. In this case, named the "global approach", the gauge's length was 300 mm (11.811 in) per side. We thus measured deformations in two directions *X* and *Y* defined by the coordinate system of the camera (Fig 1). Assuming the small strain hypothesis, the evolution of the third principal invariant of the in-plane strain tensor was physically interpreted as a surface variation parameter (dS/S) induced by the shrinkage of the cement-based material.

By considering only certain points close to the studied point, it was possible to evaluate the surface deformation field at a more local scale. Lopez has already used a pattern matching procedure to qualify strain distribution in both NSC and HPC at different creep states: in particular, this work confirmed that strain maps lead to an improved understanding of localized creep and shrinkage in concrete [11]. In the present work, a gauge length of 100 pixels/30 mm (1.181 in) was used to analyze the heterogeneity of the shrinkage at material surface. This second processing operation, named the "local approach", provided statistical analyses of the surface variation fields by computing the standard deviation of the surface variation (SD). The distribution of the SD parameter gives an idea of the strain activity at the mortar surface: indeed a high value of SD could indicate the material's ability to relax local stresses induced by shrinkage, which would delay all the early-age cracks. Another parameter was introduced; the coefficient of variation (CV), which is a normalized expression of the surface standard deviation. The coefficient of variation (CV) enables comparisons between mixtures by relative activity of local surface variation with shrinkage.

$$CV = \frac{SD}{dS/S} \quad (1)$$

Using the set of parameters established in previous works, the computation of the correlation was calibrated, giving a sensitivity of 1×10^{-5} with regard to local surface strain (dS/S).

3.1.4. Repeatability tests

The surface variation parameter obtained by the macroscopic global approach gives the free plastic shrinkage evolutions presented in Fig. 2a. The repeatability tests resulted from a (38–0–0) mixture (see Table 2). These first results show that the accuracy of the free-shrinkage test can be 2×10^{-4} until 24 h. The dispersion could be explained by the high sensitivity of plastic shrinkage to small variations in temperature and/or relative humidity. These environmental conditions can appreciably influence the drying kinetics, and consequently modify the amplitude of plastic shrinkage of cement-based materials.

Fig. 2b shows the time evolution of the deformations relative to the camera axes: although the test conditions should guarantee isotropic responses in the observed plane, one can notice in the overlapping of the *y*-axis deformation curve as anisotropic character of the shrinkage. This phenomenon could be associated to plastic relaxation as a consequence of the spreading of the mortar by the operator. However the difference between the maximum shrinkage in the two directions never exceeded 10% of the average value.

The local post-processing operation labeled the "local approach" was applied to the two previous tests. The results are presented in Fig. 3. The evolution of the local surface variation is given in terms of the standard deviation (SD) and the coefficient of variation (CV). Considerable strain activity was observed, which decreased in the first 4 h after the beginning of the test. After this initial period, a phase of stabilization is observed for these two parameters.

All these results confirm the high reproducibility of the whole experimental chain, from the mortar casting step to the deformation measurement. The standard deviation (SD) computed using the local processing operation can be associated to the shrinkage concentration phenomenon on the top surface of the mortar as shown in Fig. 4: the map of the local surface variation obtained after 10 h of drying gives an idea of the space variation of early-age shrinkage in cementitious material. Although shrinkage cracking would normally occur on the surface of the sample, the set of parameters associated with the local approach did not allow to observe them because of the low spatial resolution (30 mm gauge's length) used. In this study, the mapping of strain heterogeneity leads to only the measurement of damage extension.

3.2. Restrained plastic shrinkage test: internal stress measurement

3.2.1. Principle and conditions of test

The restrained shrinkage test is based on the ring restraining mechanism inspired by the one used by Turcry [18]. The ring of mortar was cast around a cylindrical and quasi-incompressible

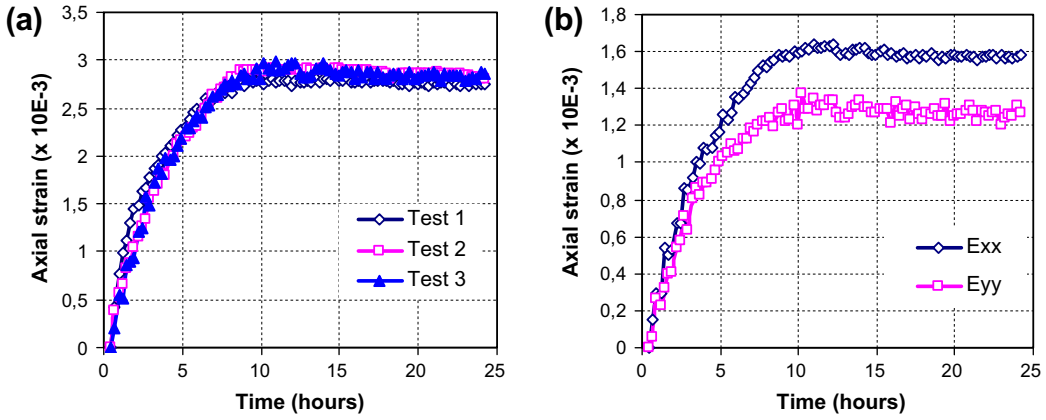

Fig. 2. Average evolution of free shrinkage during repeatability tests for the (38–0–0) mixture: evolution of the surface variation (a); anisotropic effect observed (b).

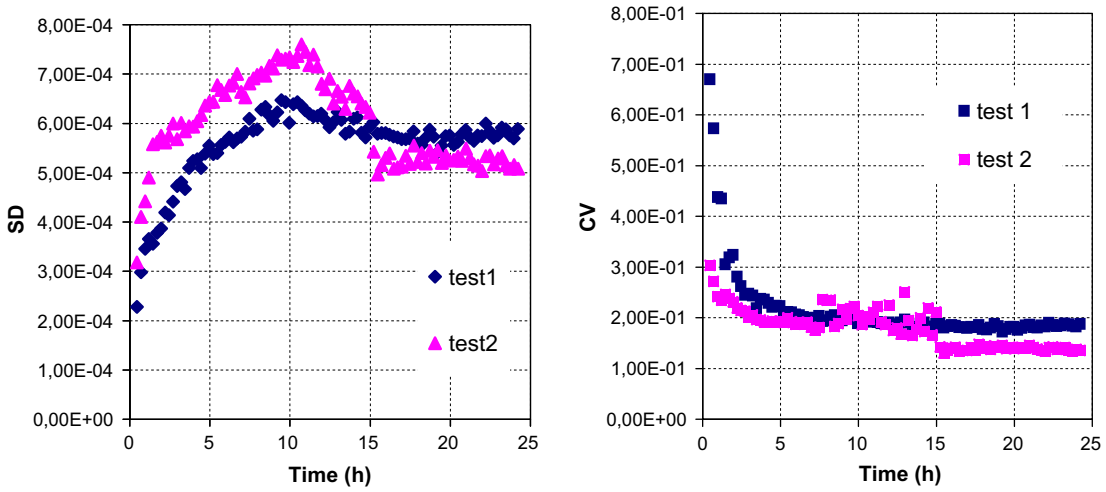

Fig. 3. Local evolution of free-shrinkage during repeatability tests: evolution of standard deviation (SD) and coefficient of variation (CV).

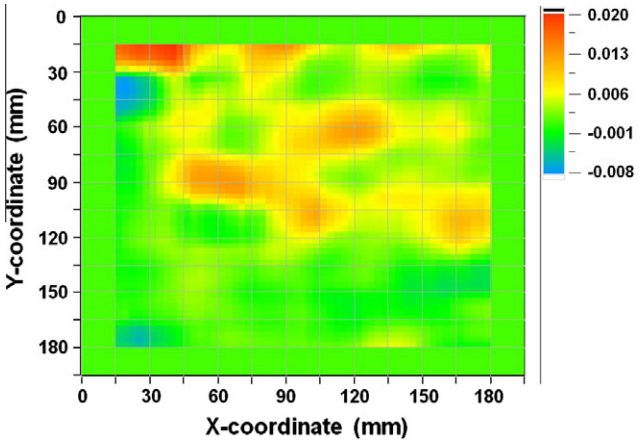

Fig. 4. Local surface variation map during free shrinkage after 10 h of drying for the (38–0–0) mixture.

polymer core (Fig. 5). The inner ring diameter, the external ring diameter and thickness of the ring sample are 320 mm (12.60 in), 400 mm (15.75 in) and 15 mm (0.59 in) respectively. The compressibility modulus of the polymer used is above 2 GPa, associated with a Poisson coefficient close to 0.5. The experimental setup was placed on a tensile-compression testing machine. As for the free-shrinkage test, this setup only enables the drying process to occur from the upper surface of mortar specimen. It could thus be assumed that that same evaporation area/volume ratio was obtained for both shrinkage tests. During the drying process, the restrained shrinkage condition of the mortar ring led to a loading of the core. This system, a computer-controlled closed loop, was an "active" system unlike the "passive" restrained shrinkage technique usually reported in the literature [8,18]. The combination of integrated displacement control in the mechanical press and a quasi-incompressible polymer core made it possible to maintain the restraining condition and core geometry during the test. The load applied to the top surface of the core, measured by the load-cell of the testing machine, revealed the evolution of the pressure induced in the core by the mortar ring during the test. The pressure in the core was directly related to the residual tensile stress ($\sigma_{\theta\theta}$) developed in the mortar ring. This corresponds to the classical problem of the thick-walled cylinder where the pressure applied to the ring inner diameter is linked by the Poisson effect to the load applied to the core. By applying the continuous medium theory, the analytical resolution of the problem in a cylindrical coordinates system is based on the assumption of plane elasticity. Each point (with a radial position R) of the mortar ring is subjected to a compressive stress and tensile stress in the radial and hoop direction respectively, as follows:

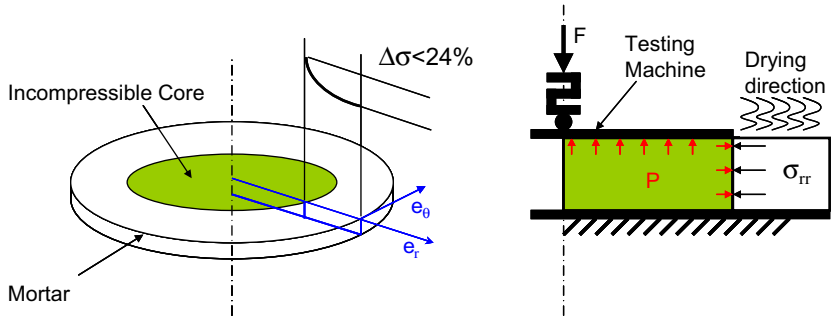

Fig. 5. Schematic representation of the active restrained shrinkage test.

$$\sigma_{rr}(R) = \frac{FR_i}{2\pi h(R_e^2 - R_i^2)}\left[1 - \frac{R_e^2}{R^2}\right]; \quad \sigma_{\theta\theta}(R) = \frac{FR_i}{2\pi h(R_e^2 - R_i^2)}\left[1 + \frac{R_e^2}{R^2}\right]. \tag{2}$$

where F, R_i, R_e and h are respectively the load measured by the cell of the testing machine, the inner radius, the external radius and the thickness of the ring.

Eq. (2) shows that the increasing stress induced in the mortar by the restraining system is not only uniaxial. Depending on the ring dimensions, a radial compressive stress (σ_{rr}) increases in the sample in addition to the rise of the tensile hoop-stress ($\sigma_{\theta\theta}$). In this study, the ring geometry was chosen to minimize the level of the radial stress. Furthermore, depending also on the geometry of the ring, the stress state is not homogenous in the sample. A tensile stress gradient is established between the outer and inner radius of the ring. The low radius ratio (R_i/R_e) of the mortar ring used in this study produced restraining conditions whose corresponding stress gradient did not exceed 24% (Fig 5). The previously mentioned common plane strain analysis gives the expression of the maximum residual hoop-stress at the inner circumference.

$$\sigma_{\theta\theta}(t) = \frac{F(t)}{2\pi h R_i}\left(\frac{R_e^2 + R_i^2}{R_e^2 - R_i^2}\right) \tag{3}$$

where $F(t)$ is the time evolution of the load during the shrinkage.

3.2.2. Calibration and accuracy tests

A calibration tests were carried out in order, on the one hand, to confirm the shrinkage restraints and, on the other hand, to verify the load transfer through the incompressible core. The previously described optical instrumentation was used to track the radial and orthoradial displacement profiles during the test. For the previous reference mortar (20–0–0) see Table 2, Fig. 6a illustrates the result obtained for a restrained shrinkage test after 10 h of drying. It was observed that the radial profile of hoop-displacements remained close to zero, except for the inner and the outer radius where boundary effects appeared to locally modify the displacement field. These results validate the required boundary conditions and that the "active" system provides a fully restrained condition.

To be sure of the load transfer through the quasi-incompressible core, a second calibration was carried out. The method consisted in measuring the mechanical properties of a hardened ring mortar whose stable properties can be considered during the calibration tests. For this purpose, For this purpose, we used the testing machine to impose a mechanical load on the core and hence on the ring mortar. The radial strain and hoop-strain were measured for an average radius using two deformation gauges laid out on the mortar in the radial and circumferential directions respectively (Fig 6b). From these measures, the associated stresses were calculated analytically by applying Eq. (2). The elastic parameters (Young's modulus E, Poisson coefficient ν) of the ring mortar are explicitly defined by the following expression:

$$E = \frac{1 - \nu^2}{\nu\varepsilon_{rr} + \varepsilon_{\theta\theta}}\sigma_{\theta\theta}; \quad \nu = \frac{K\varepsilon_{\theta\theta} - \varepsilon_{rr}}{\varepsilon_{\theta\theta} - K\varepsilon_{rr}} \quad \text{with} \quad K = \frac{\sigma_{rr}}{\sigma_{\theta\theta}} \tag{4}$$

The parameter set thus obtained was compared with those resulting from the dynamic test (resonance frequencies) applied on the same ring specimen. The resonance frequency test used is presented in Ref. [13]. Table 3 shows the Young modulus and Poisson coefficient parameters obtained by both methods. The good correlation between these results validates the complete transfer of the load using a quasi-incompressible polymeric core.

3.2.3. Repeatability tests

In order to determine the reproducibility of internal stress measurements during the restrained shrinkage test, the reference mortar (20–0–0) was tested twice. The results are presented in Fig. 7. Before the end of the dormant stage, i.e. during the first 5 h, no stress was recorded because the mortar was not stiff enough: for this stage the plastic swelling induced by the shrinkage occurred without internal stress. After the dormant stage, the tensile stress increased while a load had to be applied to the core to achieve the restrained conditions. Initially, the tensile stress increased followed by a slight decrease. These repeatability tests show that the sensitivity of the restraining stress is better than ±0.002 MPa.

The lower level of stress attained during the period of the early-age under study (less than a few percent of MPa), requires highly accurate measurements of both the displacement and load associated with the active system. Passive systems, which tolerate shift with fully restrained conditions, are used to study drying shrinkage over several days and are mostly associated with higher level of stress [8,18].

4. Experimental results and discussion

4.1. Free early-age shrinkage results

4.1.1. Effect of cellulose ether on free early-age shrinkage

Fig. 8a shows the effect of cellulose ether on the evolution of the surface strain during free plastic shrinkage tests. Reducing the quantity of cellulose ether modifies the kinetic and level of early-age shrinkage. For 0.38% of cellulose ether, the shrinkage curve presents two stages: a transitional stage where the shrinkage speed decreases gradually, followed by an asymptotic stage. The shrinkage induced by the capillary depression seems to be gradually compensated by the cement-based setting phenomenon. For 0.20% of cellulose ether, the kinetic occurs in three stages. In a first stage, i.e. 7 h, the early-age shrinkage is reduced by a third with regard to the mortar (38–0–0). Reducing the rate of cellulose ether

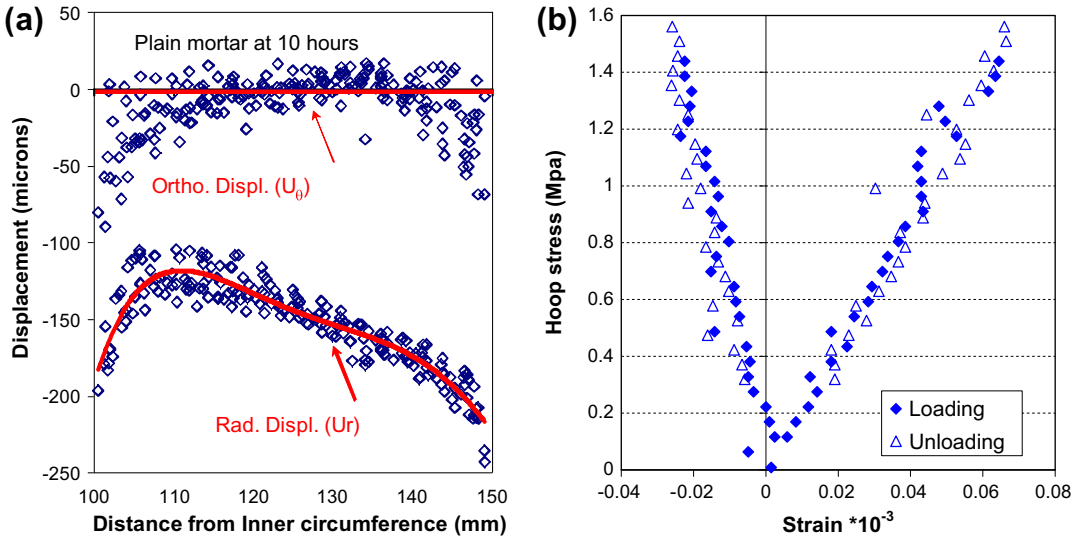

Fig. 6. Restrained shrinkage calibration test: radial profiles of the radial and hoop displacements during shrinkage test (a) stress–strain response of the ring under loading (b).

Table 3
Comparison of the two measurement techniques.

	Resonance frequencies method	Static method (gauge)
E (GPa)	22.8	21.6
v	0.22	0.28

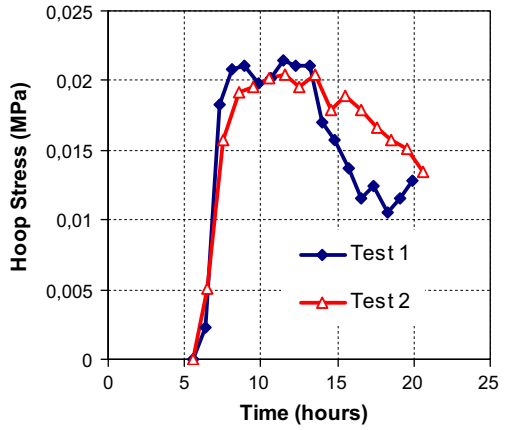

Fig. 7. Restraining stress evolution during repeatability tests for the (20–0–0) mixture.

reduces the initial granular interaction in the fresh mortar. This result shows the importance of the rheology of fresh mortar with regard to early-age shrinkage development, as has already been observed in the literature [18]. The first stage preceded the settlement of the mortar checked with needle penetration tests (Vicat test). The first stage was followed by a sudden rise and then stabilization of the shrinkage. Contrary to the previous effect, the level reached at the asymptotic stage was reduced by an increase in the cellulose ether rate. The shrinkage kinetic observed in the second transitional stage was faster for the 0.20% CE mortar than the 0.38% CE mortar. The same difference is also observed regarding the kinetic of the evaporation rate for both formulations (Fig. 8b). This result is in agreement with the literature: the addition of cellulose ether decreases the early-age evaporation rate of cement-based materials [20].

4.1.2. Effect of EVA and glass fibers on free plastic shrinkage

The effect of substituting part of the sand by a polymer powder (EVA) and/or the addition of glass fibers were also studied. The 0.20% cellulose ether formulation was used as reference mortar (20–0–0). A considerable decrease in shrinkage was observed for the mortar modified with EVA (20–2–0) by comparison with the reference mortar (Fig. 9a). Two concomitant effects could explain this phenomenon: the first is that hydrates produced during the first stage (during which the shrinkage kinetic slows down) are mixed with dispersed EVA particles to constitute a co-matrix phase [14]. This co-matrix gives an "apparent cohesion" of the fresh mortar and thus contributes to the decrease in early-age shrinkage. The second explanation is that, at the first stage, drying from the open surface of the mortar contributes to polymer layer formation on the top surface of the mortar: the polymer particles (EVA) dispersed in the cementitious matrix migrate and generate the fast formation of a polymer layer which seals the sample and reduces the early-age shrinkage [14].

Fig. 9b illustrates the influence of glass fibers on surface strain evolution during the free-shrinkage test. By comparison with the reference mortar (20–0–0), the GF formulation (20–0–6) shows a major reduction in early-age shrinkage. During mixing, the glass fibers break into many individual fibers filaments which are dispersed uniformly in the mortar. These individual fibers filaments provide suitable micro-reinforcement because of their favorably high specific surface. The bonding between the fibers filaments (polypropylene and glass fibers in particular) and the mortar matrix develops quickly [3,6]. Thus, from a macroscopic point of view, the early-age shrinkage could be reduced by adhesion between the glass fibers filaments and the cementitious matrix. The tangential strength contributed by the fibers is commonly attributed to the better mechanical properties of the fibers compared with the cementitious matrix [17,23].

Fig. 9c and d shows the evolution of the statistical parameters (SD and CV) obtained by the local approach described in Section 3.1. As mentioned above, the standard deviation (SD) is associated to the local shrinkage concentration phenomenon on the surface material. This statistical parameter enables the heterogeneity of the early-age shrinkage to be visualized. The results presented in Fig 9c indicate that the glass-fiber reinforced mortar showed more homogeneous surface shrinkage than the other formulations. This strain activity reported to the average shrinkage gives the coefficient of variation (CV). The relative shrinkage activity given by the CV evolution is shown in Fig. 9d. After

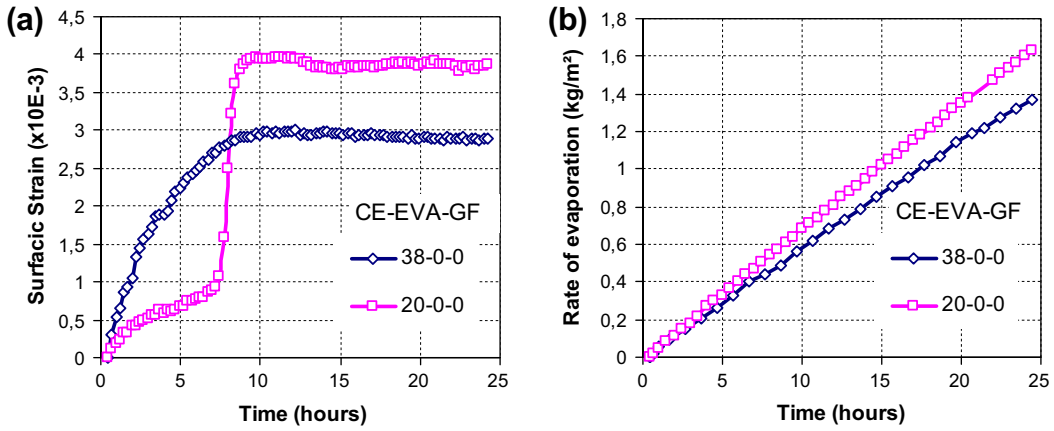

Fig. 8. Effect of cellulose ether on free shrinkage (a) and associated water loss (b).

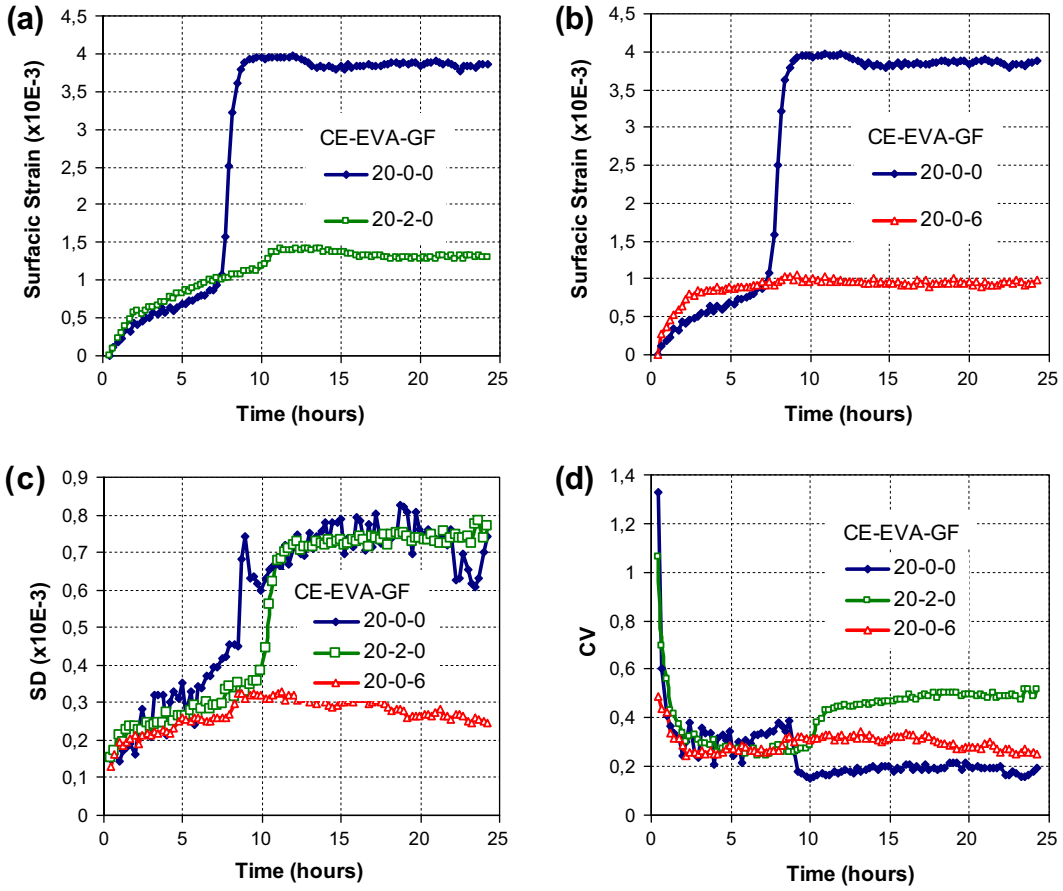

Fig. 9. Influence of EVA and glass fibers on free shrinkage.

10 h, which approximately corresponds to the initial Vicat setting time, all the formulations had stabilized, although at different levels. If an increase in the CV parameter after settlement leads to the growth of local internal stress and thus to early-age cracks, all the formulations tested in this study are promising from this point of view.

4.2. Restrained early-age shrinkage results

4.2.1. Effect of EVA and glass fibers

The restrained shrinkage test associated to an active system enables measurement of the tensile stress developed in the cement-based material during drying. All the tests were performed under the same environmental conditions as for the previous free plastic shrinkage tests. The results obtained for the three formulations are presented in Fig. 10. For each formulation, restrained tensile stress starts to evolve only after the corresponding first stage observed with the free-shrinkage tests. Indeed, during the dormant stage, the mortar can be regarded as a non-rigid paste. Fig. 10a shows the results related to the EVA modified mortar (20–2–0). One can notice a delay in the tensile stress evolution of the EVA modified mortar by comparison with the reference mortar (20–0–0). This is undoubtedly related to the influence of EVA on the kinetics of mortar cohesion. The

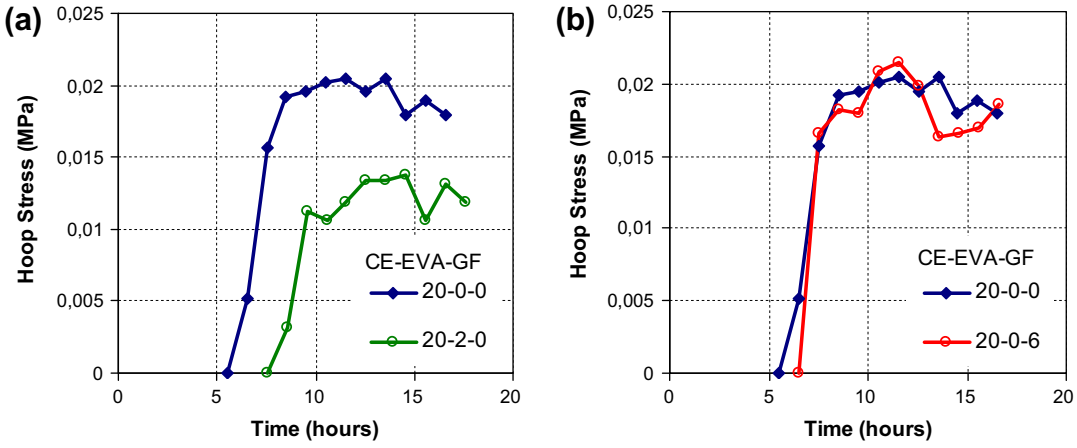

Fig. 10. Influence of EVA (a) and glass fibers (b) on restrained tensile stress.

use of EVA increases the dormant period of cementing materials [14].

After this dormant stage, the simultaneous evolution of the mortar cohesion and the drying shrinkage resulted in the increase of tensile stress in the mortar. The residual restrained tensile stress increased until a certain level followed by stabilization. Although it was for autogenous shrinkage some recent studies reported similar behavior in the literature concerning early-age behavior of high strength mortar during restrained shrinkage tests [9,15]. After stabilization, the restrained tensile stress decreased until the end of the test. This slight decrease in tensile stress could be related to the creep phenomenon which is very important at the early age when the mortar is subjected to restrained shrinkage. Also in Fig. 10, note that the reference mortar (20–0–0) reached a relatively low level of tensile stress (0.02 MPa) during the restrained shrinkage test. The poor mechanical characteristics of this mortar (its compressive strength is 12.2 MPa at 28 days) could explain this low level of the tensile stress.

In Fig. 10a, we also observe that the EVA modified mortar reached a low tensile stress level compared to the reference mortar. Two concomitant effects could be explain this result. Firstly, as mentioned above, the EVA modified mortar showed low shrinkage (Fig. 9a). Secondly, EVA modified mortar generally shows low rigidity [12,14].

Fig. 10b shows the influence of glass fibers (0.035% by volume or 0.06% by weight) on the evolution of restrained tensile stress. We observe that the GF mortar (20–0–6) has the same kinetic evolution and level of residual tensile stress as the reference mortar under the same restraining conditions. Furthermore, as seen in Fig. 9b, the FG reinforced mortar showed a very large reduction in both surface shrinkage level and local strain activity compared to the other mixtures. All the characteristics obtained with both the restrained and free-shrinkage tests seem to indicate that the addition of glass fibers is the most effective means of alleviating the risk of cracking.

5. Conclusion

This work deals with the shrinkage of thin sheets of mortar (such as pavements or facings) under early-age drying conditions. An original experimental procedure was developed to investigate early-age shrinkage using a free-shrinkage test (a slab test), and an active restrained shrinkage test (a ring test).

Because early-age cracks are the first damage to appear on the drying surface, the evolution of the shrinkage strain at the open surface of the slab test was investigated using an optical instrumentation system. This technique involved the evaluation of the in-plane kinematic surface field without contact with the tested sample during the free-shrinkage test. In addition to a global approach with regard to the evolution of the shrinkage strain over the entire drying surface, statistical parameters were defined in a local approach to analyze the strain distribution at the surface. In particular, strain maps generated by this technique provided interesting data on the mortar's ability to relax local stresses induced by the shrinkage. The restrained shrinkage test used an original and simple active system which continuously produced restrained conditions throughout the test. This experimental technique provided accurate quantitative information on the development of very early-age tensile stress.

The whole experimental procedure enabled comparison of the various formulations and the effects of shrinkage reduction agents. The effects of glass fiber and EVA polymer were investigated. Results showed that glass fibers do not modify the increase in the restrained tensile stress compared to the unmodified formulation but drastically reduce the free shrinkage and local strain activity at the drying surface of the mortar. Both these results could explain the better effect of glass fibers with regard to cracking risk of concretes. A similar conclusion was observed by Schwartzentruber et al. for glass-fiber reinforced (1% by volume) ultrahigh strength mortar [15]. The addition of EVA polymer reduces the mortar cohesion evolution kinetic, which leads to a delay in the tensile stress evolution and a lower maximum stress level.

By investigating the consequences of both drying shrinkage due to evaporation and restrained conditions on the cracking potential of mortar mixtures, the information obtained by the experimental procedure presented in this work has provided interesting quantitative data.

References

[1] Acker P, Michaud-Pourpadin V. Limiter la fissuration: Conditions indispensables à la durabilité des structures en béton. Bulletin des laboratoires des ponts de chaussées 238, Mai-Juin 2002;4433:13–24.
[2] Baron J. Les fissurations spontanées et accidentelles du béton non armé et armé. Le béton hydraulique, Paris, Press de l'ENCPC; 1986. p. 503–12.
[3] Bayasi Z, Mclntyre M. Application of fibrillated polypropylene fibers for restraint of plastic shrinkage cracking in Silica fume Concrete. ACI Mater J 2003;99(4):337–44.
[4] Dias WPS. Influence of mix and environment on plastic shrinkage cracking. Mag Concr Res 2003;55(4):358–94.
[5] Giton M, Ienny P. Amélioration des performances de mesure de déformation par extensiométrie optique bidimensionnelle. Compte rendu du Colloque Mécamat 2001:196–9.
[6] Hardmeler S, Stahltoo AG. AR glass fibers as microreinforcement to limit crack formation and increase strength of floor screed and concrete. In: Asia-pacific conference on fiber reinforced concrete, Singapore, August 28–29; 1997.

[7] Holt E, Leivo M. Cracking risks associated with early age shrinkage. Cement Concr Compos 2004;26(5):521–30.
[8] Hossain AB, Weiss J. Assessing residual stress development and stress relaxation in restrained concrete ring specimens. Cement Concr Compos 2004;26(5):531–40.
[9] Igarashi S, Bentur A, Kovler K. Autogenous shrinkage and induced restraining stress in high-strength concretes. Cement Concr Res 2000;30:1701–7.
[10] Laraba-abbes F, Ienny P, Piques R. A new tailor-made methodology for the mechanical behaviour analysis of rubber-like materials: I. Kinematics measurements using a digital speckle extensometry. Polymer 2003;44:807–20.
[11] Lopez M, Khan LF, Kurtis KR. Characterization of elastic and time-dependent deformations in normal strength and high performance concrete by image analysis. Cement Concr Res 2007;37:1265–77.
[12] Messan A. Contribution à l'étude du comportement au très jeune âge des structures minces en mortier. PhD thesis. Université de Montpellier 2; 2006.
[13] Messan A, Corn S, Ienny P. Composites cimentaires: endommagement et maturation suivis par analyse vibratoire. Rev des Compo et des Mat Av 2007;17(2):239–50.
[14] Ohama Y. Principe of latex-modified mortars and concretes. ACI Mater J 1987;84(6):511–8.
[15] Schwartzentruber A, Philippe M, Marcheses G. Effect of PVA Glass and metallic fibers, and of an expansive admixture on the cracking tendency of ultrahigh strength mortar. Cement Concr Compos 2004;26:573–80.
[16] Slowik V, Schlattner E, Klink T. Experimental investigation into early age shrinkage of cement past by using fibre Bragg gratings. Cement Concr Compos 2004;26(5):473–9.
[17] Toledo Filho RD, Ghavami K, Sanjuàn MA, England GL. Free, restrained and drying shrinkage of cement mortar composites reinforced with vegetable fibres. Cement Concr Compos 2005;27(5):537–46.
[18] Turcry P. Retrait et fissuration des bétons autoplaçants: influence de la formulation. PhD thesis, Ecole Centrale de Nantes et Université de Nantes; 2004.
[19] Uno PJ. Plastic shrinkage cracking and evaporation formulas. ACI Mater J 1998;95(4):365–7.
[20] Vallee F. Durabilité des composites polymères/ciment: application au cas des enduits minces sur les isolants. PhD thesis. Institut National Polytechnique de Grenoble; 1999.
[21] Wang K, Shah SP, Phuaksuk P. Plastic shrinkage cracking in concrete materials – influence of fly ash and fibers. ACI Mater J 2001;98(6):458–64.
[22] Wong Allan CL, Childs PA, Berndt R, Macken T, Peng GD, Gowripalan N. Simultaneous measurement of shrinkage and temperature of reactive powder concrete at early-age using fibre bragg grating sensors. Cement Concr Compos 2004;29:490–7.
[23] Zhang J, Li VC. Influences of fibres on drying shrinkage of fibre reinforced cementitious composites. J Eng Mech 2001;127(1):37–44.